Scientific Reports

https://doi.org/10.1038/s41598-026-62583-3

Article in Press

Transcranial functional ultrasound imaging shows widespread hemodynamic changes induced by focused ultrasound (FUS)

Received: 16 October 2025

Accepted: 13 July 2026

Published online: 21 August 2026

Cite this article as: Bendig J., Aurup C., Blackman S.G. *et al.* Transcranial functional ultrasound imaging shows widespread hemodynamic changes induced by focused ultrasound (FUS). *Sci Rep* (2026). https://doi.org/10.1038/s41598-026-62583-3

Jonas Bendig, Christian Aurup, Samuel G. Blackman, Erica P. McCune, Seongyeon Kim & Elisa E. Konofagou

Transcranial Functional Ultrasound Imaging Shows Widespread Hemodynamic Changes Induced by Focused Ultrasound (FUS)

Jonas Bendig[1*], Christian Aurup[1*], Samuel G. Blackman[1], Erica P. McCune[1], Seongyeon Kim[1], and Elisa E. Konofagou[1,2,3]

*These authors contributed equally

[1]Department of Biomedical Engineering, Columbia University, New York, NY, USA

[2]Department of Radiology, Columbia University, New York, NY, USA

[3]Department of Neurosurgery, Columbia University, New York, NY, USA

Correspondence to: Elisa E. Konofagou and Jonas Bendig
Full address: 630 West 168th Street, New York, NY 10032, USA
E-mail: ek2191@columbia.edu; jb4781@columbia.edu

Abstract

Background: Focused ultrasound (FUS) is an emerging non-invasive technique to induce a variety of biological effects in the central nervous system (CNS). Functional ultrasound imaging (fUSI) leverages ultrafast Power Doppler Imaging (PDI) to detect changes in cerebral blood volume (CBV) and thus hold promise to monitor brain responses to FUS. An integrated, non-invasive, ultrasound-based system for transcranial mapping of FUS responses could help elucidate the physiological effects of FUS in the brain and provide both feedback and understanding of the underlying mechanism.

Objective: To demonstrate the feasibility of transcranial fUSI to characterize the immediate and short-term hemodynamic effects of transcranial FUS stimulation in the mouse brain.

Methods: We used a co-aligned FUS-fUSI system to apply FUS and transcranially monitor hemodynamic changes during and immediately after stimulation in lightly anesthetized mice. We investigated the effects of varying intensities and transducer positions on the hemodynamic responses.

Results: We found widespread hemodynamic responses not confined to the focal area and show that higher FUS pressures increase the size of the brain area with a significant hemodynamic

response, as well as the magnitude of change in CBV. Sham sonications, as well as FUS with lower pressures did not induce hemodynamic responses and unilateral sonications resulted in bilateral hemodynamic changes with a significantly stronger response on the ipsilateral side. FUS stimulation in mice with a cranial window showed distinct activation patterns that were frequency-dependent and different from the activation patterns observed in the transcranial model. Specifically, the widespread cortical response observed transcranially was substantially reduced in the window model, indicating that skull-mediated thermal effects are a primary driver of the cortical hemodynamic changes observed in the transcranial condition.

Conclusion: fUSI is shown capable of transcranially monitoring online and short-term hemodynamic effects in the brain during and following FUS stimulation.

Keywords: Focused Ultrasound (FUS), Neuromodulation, Transcranial, Functional Ultrasound (fUSI), Hemodynamic Response, Power Doppler

Introduction

Focused ultrasound (FUS) has shown the ability to induce a range of biological effects in the central nervous system (CNS), which include neuromodulation [1–9], changes in astrocytic and microglial function [10–12] or vascular effects [13–15]. The specific outcomes are highly dependent on the acoustic parameters; while mainly low-intensity FUS has been explored for neuromodulation a variety of studies has demonstrated potent neuromodulatory effects without tissue damage with comparatively higher FUS pressures or intensities [16–20]. Especially in FUS with higher intensities, temperature increases become likely contribute to the overall biological effects and have been shown to induce neuromodulation [21–24]. Against the background of the diverse effects of FUS in the CNS, more direct measurements of FUS induced effects in the brain

are needed to fully assess the acute and long-term effects of FUS in the targeted area as well as connected brain regions.

Functional magnetic resonance imaging (fMRI) [25,26] is the most common techniques for studying neuronal activity or changes in blood flow in the CNS in animal models and humans. However, fMRI requires long imaging sessions in a spatially confined MRI scanner with high capital costs [27–29]. In contrast, functional ultrasound imaging (fUSI) is an emerging imaging technique [30–32] that allows monitoring of stimulus-evoked activity, functional connectivity and potential changes in blood flow in the whole brain with a comparatively small ultrasound array [33–36]. fUSI uses ultrafast Power Doppler Imaging (PDI) to measure changes in cerebral blood volume while suppressing signals from the surrounding tissue through the implementation of advanced spatiotemporal filtering techniques such as singular value decomposition (SVD) [37,38]. Analogous to fMRI, fUSI leverages neurovascular coupling and has been shown to correlate well with neuronal activity and local field potentials [39,40]. The spatial resolution is similar to that of fMRI [41] but it attains greater temporal resolution [27]. fUSI typically achieves temporal resolutions on the order of hundreds of milliseconds. In the present study, the effective temporal resolution was approximately 1 s (one compound Power Doppler frame per second).

The principal challenge in applying transcranial fUSI to the brain is the substantial acoustic attenuation induced by the skull. Consequently, most implementations of fUSI to date have relied on the removal or thinning of the skull bone [29]. Previous work by our group and others has demonstrated transcranial applications of fUSI for detecting hemodynamic changes in the mouse brain [34,42–44], allowing for a fully noninvasive ultrasound-based functional brain imaging technique. In addition, we have recently demonstrated the feasibility of a combining fUSI with FUS stimulation in craniotomized mice [45]; however, the requirement of a non-survival and

highly invasive, head-wide craniotomy prohibits widespread acceptance and limits potential applications as well as translatability. Achieving transcranial fUSI in combination with FUS could allow noninvasive stimulation while monitoring the resulting bio-effects in a large field of view and potentially allow further translation of the technique.

In this study, we employed a simultaneous, transcranial FUS and power Doppler imaging configuration to assess the immediate and short-term hemodynamic effects of transcranial FUS stimulation. Crucially, the acoustic parameters utilized in the present study (i.e. peak negative pressures and intensities) span from lower to higher intensity regimes and mostly exceed the values commonly used in low-intensity ultrasound neuromodulation studies. We demonstrate that the size of the area with significant hemodynamic responses and the change in cerebral blood volume (CBV) are positively correlated with the magnitude of the applied pressure and that unilateral sonications result in bilateral hemodynamic changes with a significantly stronger response on the ipsilateral side. Importantly, transcranial FUS is shown to induce hemodynamic changes in widespread brain regions, not necessarily located within the focal area. FUS neuromodulation in mice with a cranial window shows distinct patterns of CBV changes that were frequency-dependent and different from the patterns observed in the transcranial model. While FUS with higher intensities caused consistent hemodynamic responses, lower intensities that are commonly used in low intensity ultrasound neuromodulation studies were not able to elicit significant hemodynamic responses detectable with fUSI.

Results

fUSI transcranially detects hemodynamic responses during and following FUS

To investigate if transcranial FUS with a center frequency of 1.68 MHz can induce a hemodynamic response in the mouse brain, we utilized transcranial fUSI with a transmit frequency of 15 MHz

and compared active FUS with two sham conditions: Sham trials performed with the amplifier powered off showed no significant changes in CBV (6 mice, 22 trials in total, transcranially, Figure 1 c/d). Similarly, an auditory sham condition with a 110 dB loud 10 kHz tone (n = 3 mice, implanted with a cranial window, Figure 1 e/f) showed no CBV changes. However, FUS routinely produced widespread hemodynamic responses in sonicated subjects in the transcranial ($p < 0.0001$ vs sham, Wilcoxon signed-rank test) and cranial window conditions. Activity was typically observed both within the focal region and across the cortex in both hemispheres.

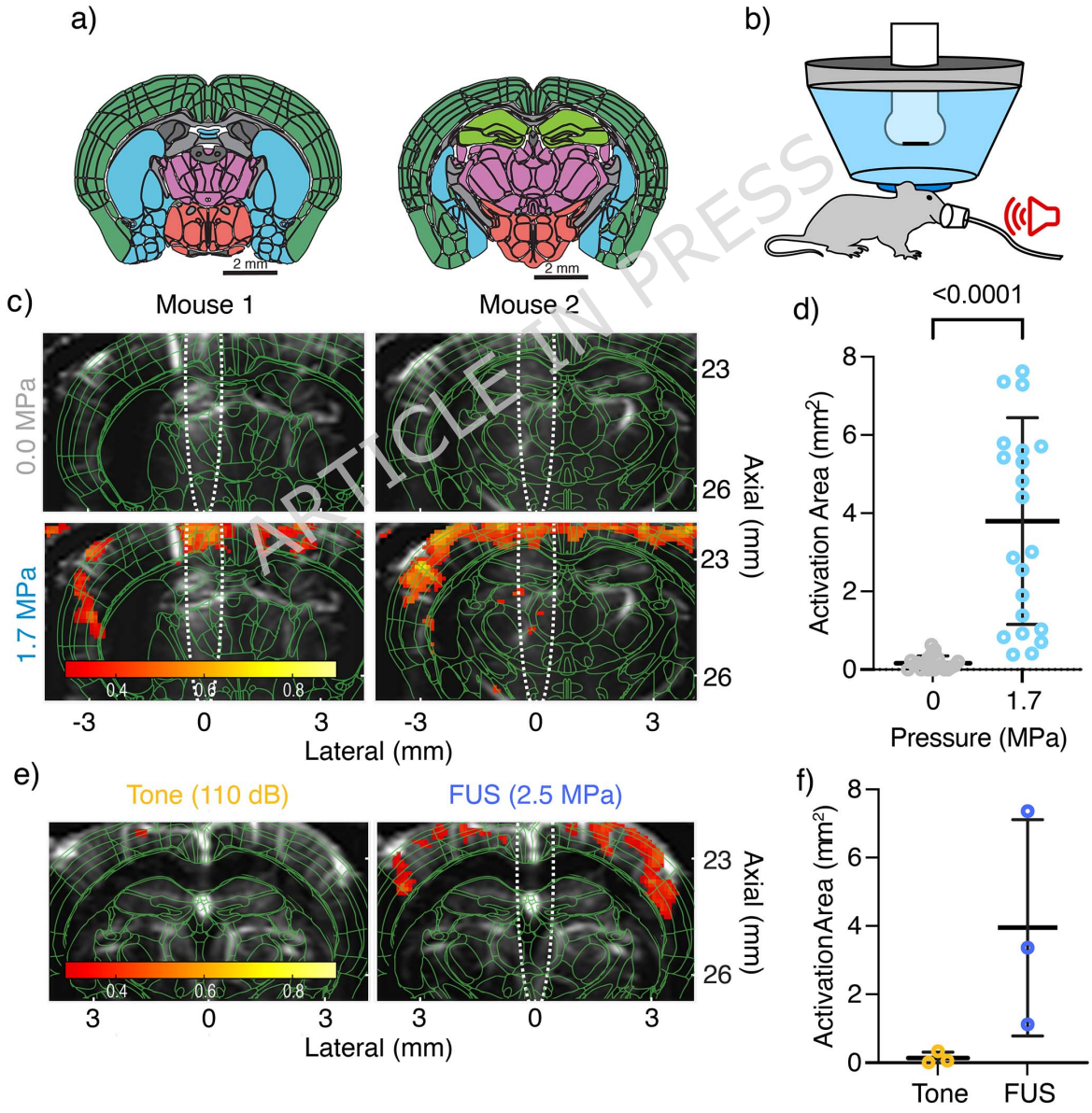

Figure 1. Hemodynamic response in FUS (center frequency: 1.68 MHz) and sham trials. **(a)** Schematic representation of the imaging planes in **b** (left: Mouse 1, AP Bregma – 0.6 mm; right: Mouse 2, AP Bregma – 1.4 mm) and c (right, AP Bregma – 1.4 mm) and. Brain regions are colored analogous to the Allen Mouse Brain Atlas [46] (Cortex: Dark green, Cerebral nuclei: Blue, Hippocampus: Light green, Thalamic nuclei: Purple, Hypothalamic nuclei: Red, Fiber tracts: Light gray, Ventricular System: Dark gray). **(b)** Schematic representation of the setup used for sham/active trials (Functional ultrasound transducer: White, FUS transducer: Gray, Water-filled coupling cone: Light blue, Coupling gel: Dark blue, Speaker: Red). **(c)** Activity maps of two subjects receiving FUS-Off sham and active FUS conditions overlaid onto PDI (grayscale) and brain regions (green). The predicted acoustic focus assessed during transducer calibration is overlaid with a white dotted line. Activity maps display the full extent of the imaging field of view; the dorsal cortex near the midline is outside the imaging plane due to the trade-off between field of view and temporal resolution. **(d)** Wilcoxon matched-pairs signed rank test revealed a significantly greater area with CBV increases correlated with the FUS stimulus in the FUS group (n = 22 paired trials in 6 mice, median AP direction of imaging planes: -0.75 mm from Bregma, Range = -0.5 mm to -1.4 mm). **(e)** Representative activity maps for a subject receiving auditory stimulation only (tone) and active FUS overlaid onto PDI (grayscale) and brain regions (green). **(f)** Comparison of areas of CBV increases correlated with the FUS stimulus for auditory stimulation and active FUS condition (n = 3 paired trials in 3 mice, median AP direction of imaging planes: -1.5 mm from Bregma, Range = -1.4 mm to -1.6 mm). Data in panels c/d is based on transcranial imaging, while data in e/f was obtained in mice with cranial windows. Graphs depict individual observations (circles) with mean (central line) and standard deviations (whiskers). Activity maps and color bars show Spearman correlation coefficients. Only significantly correlated pixels (Spearman's $\rho > 0.285$ are displayed)

Hemodynamic responses in the brain depend on FUS pressure

To determine whether response patterns depend on the applied acoustic pressure, 4 subjects were sonicated with 3 different FUS pressures in randomized order for a total of 10 trials (n = 4 trials

for 1 subject, n = 3 trials for 1 subject, n = 2 trial for 1 subject and n = 1 trial for 1 subject) and hemodynamic changes were detected with transcranial fUSI. A sample of pressure conditions for 3 subjects is provided in Figure 2 a.

We found a significant difference between the area of CBV increases correlated with the FUS stimulus for different pressure groups ($p = 0.0063$, Friedman test) with the highest pressure of 2.6 MPa causing CBV increases in a significantly greater area compared to the 0.8 MPa group ($p = 0.0177$, Wilcoxon matched-pairs signed rank tests with Bonferroni correction, Figure 2 c). To further investigate the effects of pressure on the CBV response, we calculated the mean CBV change over time in all jointly significantly correlated pixels that were common to each of the three pressure conditions in individual trials (2 trials were omitted from the analysis because the 0.8 MPa condition did not yield any significance). We found a significantly higher maximal CBV increase in the 2.6 MPa group compared to the 0.8 MPa group ($p = 0.0278$, Wilcoxon matched-pairs signed rank test with Bonferroni correction, after significant Friedman test ($p = 0.0303$), Figure 2 d).

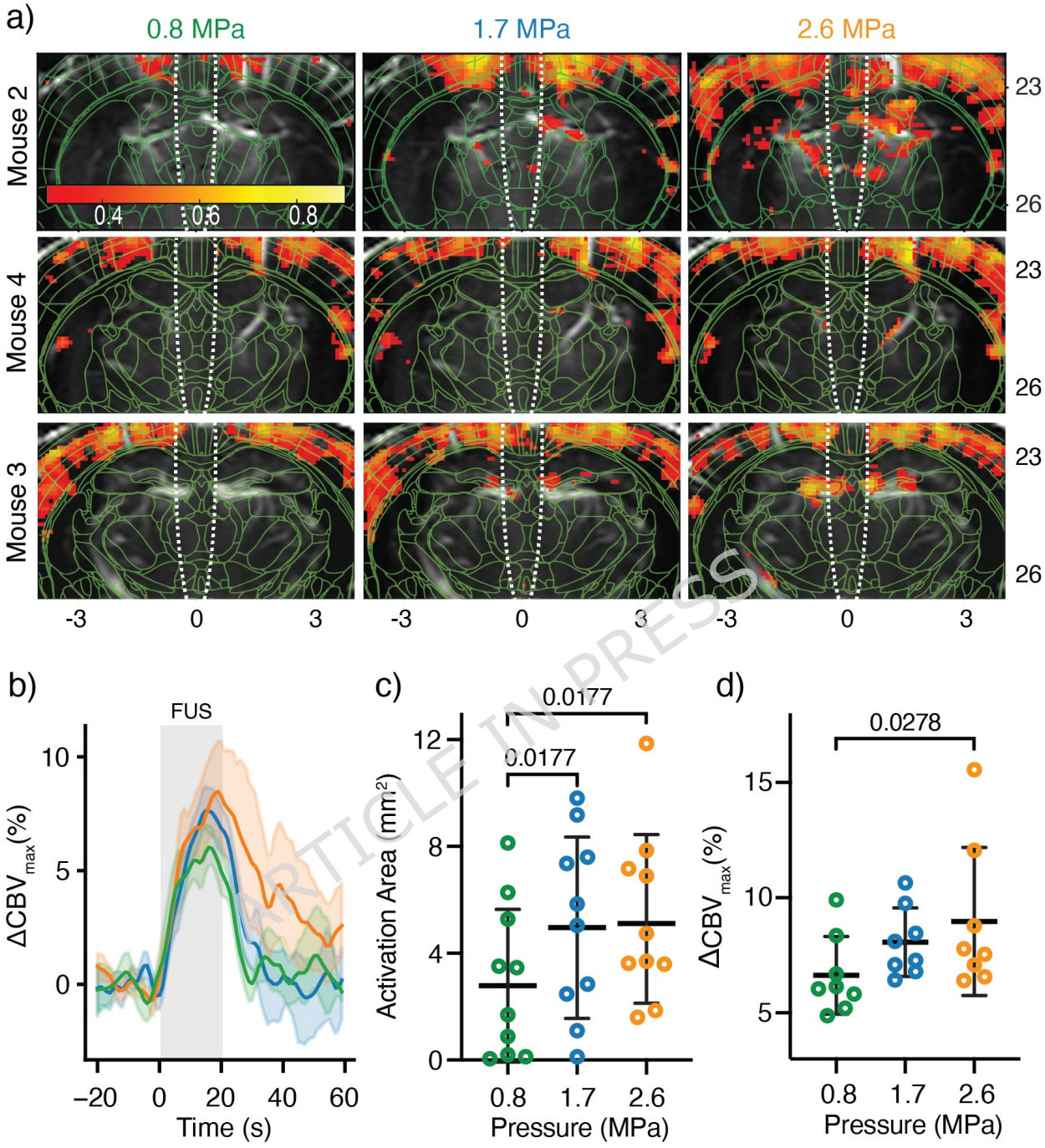

Figure 2. Higher pressures of transcranial FUS (center frequency: 1.68 MHz) induce greater activation in mice. **(a)** Activity maps of significantly correlated pixels (Spearman's $\rho > 0.285$) overlaid onto PDI (grayscale) and brain regions (green) for 3 subjects receiving 0.8, 1.7, and 2.6 MPa FUS. Predicted acoustic foci (white, dotted line) assessed during transducer calibration are overlaid onto the images. Imaging planes:

Upper row AP Bregma -0.5 mm, middle row AP Bregma -1.0 mm, bottom row AP Bregma -1.5 mm; Different imaging planes are shown to demonstrate that pressure-dependent effects are consistent across coronal planes. The anteroposterior (AP) position of the imaging plane varied across animals due to manual positioning of the imaging transducer and the approximately 400 μm thickness of the imaging plane in the AP direction. Activity maps display the full extent of the imaging field of view; the dorsal cortex near the midline is outside the imaging plane due to prioritization of temporal resolution over field of view. **(b)** Mean CBV changes (solid) and 95% confidence interval for all jointly significantly correlated pixels across all trials (n = 8 paired trials in 4 mice, no pixels found in 2 trials). Multiple Wilcoxon matched-pairs signed rank tests (with Bonferroni correction, after significant Friedman tests: $p = 0.0063$ **(c)** and $p = 0.0303$ **(d)**) revealed significantly greater areas of CBV increases correlated with the FUS stimulus **(c)** and peak CBV changes in jointly significant pixels **(d)** as pressure increased (n = 10 paired trials in 4 mice, no jointly significant pixels in 2 trials, median AP direction of imaging planes: -1.0 mm from Bregma, Range = -0.2 mm to -1.5 mm). Data is depicted as individual observations (circles) with mean (central line) and standard deviations (whiskers). Activity maps and color bars show Spearman correlation coefficients.

CBV changes are not confined to the FUS focus and more pronounced in cortical areas

Next, we assessed the spatial distribution of hemodynamic changes by comparing CBV changes within the FUS focus and the surrounding off-focus tissue across anatomical regions (Figure 3). The magnitude of the CBV responses (mean of CBV change during FUS) was not significantly different between the in-focus and off-focus zones (Two-way ANOVA, $p = 0.5137$). However, we observed that CBV responses in cortical areas were substantially greater than those in both sub-cortical and deeper brain structures ($p = 0.0380$ and $p = 0.0001$, respectively; Dunn's test after significant Friedman test ($p < 0.0001$)). The time-course data further confirms that this widespread effect, characterized by a dominant cortical response, was a consistent feature especially in higher FUS pressures (Figure 3 c-e).

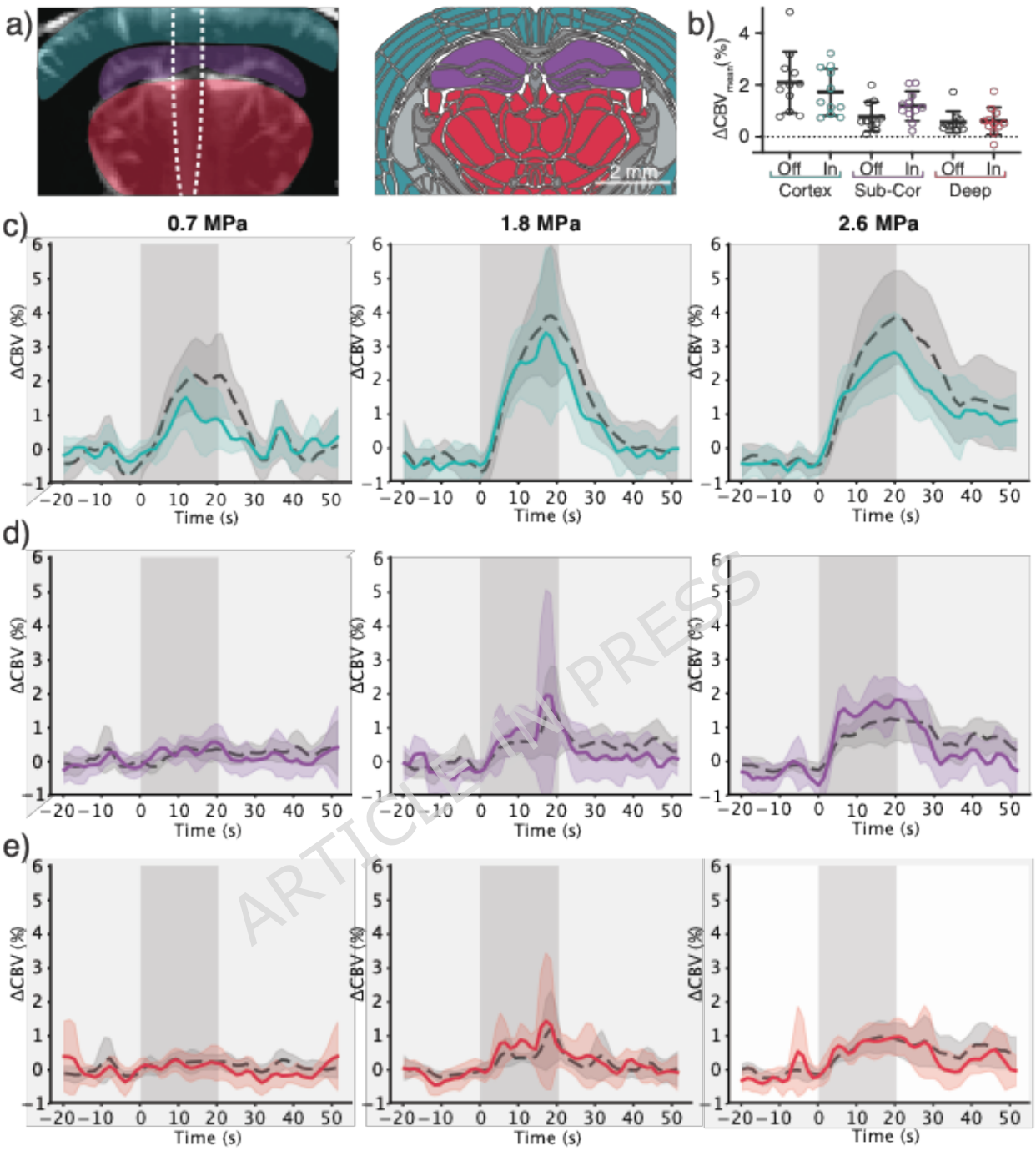

Figure 3. Comparison of CBV changes in- and off-focus in different brain areas with transcranial FUS (center frequency: 1.68 MHz). **(a)** Regions of interest (ROIs) that were used in the analysis overlaid onto a Power Doppler Image and the schematic representation of brain regions from the Allen Mouse Brain Atlas [46]: Teal – Cortical areas; Orchid – Hippocampus, Fimbria and ventral hippocampal commissure; Red – Thalamus and Hypothalamus. The dotted white line shows the predicted acoustic foci (white) assessed

during transducer calibration. **(b)** Mean CBV changes during the FUS neuromodulation period in the ROIs shown in (a) separated for in- and off-focus activity at 2.6 MPa derated PNP. There were no significant differences between in- and off-focus CBV changes (Two-way Anova: $p = 0.8948$ for in- vs off-focus and $p = 0.2252$ for interaction term of focus with brain region), but significantly more CBV increase (mean of CBV increase during FUS window) in the cortical regions (Cortex vs Sub-Cortex: $p = 0.0380$; Cortex vs deep regions: $p = 0.0001$; Dunn's test after significant Friedman test ($p < 0.0001$)). (**c/d/e)** Time traces of in- and off-focus CBV changes in cortical (c), sub-cortical (d) and deeper brain regions (d) with different FUS pressures (columns). Colored lines represent in-focus CBV changes and dashed black line off-focus CBV changes. Shaded areas show 95% confidence interval. The grey bar between 0 and 20 s represents the duration of FUS neuromodulation.

Non-Transcranial FUS shows distinct CBV responses

To investigate possible effects of the skull on the response patterns, FUS was delivered with different pressures in 5 mice implanted with cranial windows. We further evaluated possible effects of frequency and focal size by using a 4 MHz transducer to deliver FUS with comparable pressures. Like the transcranial condition, there were significant differences between the pressure groups for both tested frequencies (Friedman test, 1.68 MHz: $p = 0.0010$, 4.0 MHz: $p < 0.0001$). We found significantly larger areas of CBV increases correlated with the FUS stimulus in 2.8 MPa FUS compared to the lower pressures in the 1.68 MHz condition (Figure 4 b). Similarly, with 4 MHz FUS the area that showed CBV increases correlated with the FUS stimulus was significantly larger compared with higher pressures (Figure 4 c). Clear trends for an increase in CBV start at pressures of 2.1 MPa in the 1.68 MHz condition and at 1.8 MPa in the 4 MHz condition (Figure 4 b/c). Compared to transcranial FUS there was no activation in lower pressure conditions. Especially in lower pressures, cortical CBV increases correlated with the FUS stimulus were less pronounced in mice with cranial windows, while subcortical responses appeared enhanced (Figure

4 a). Interestingly, we found significant negative correlations in the cranial window condition (Figure 4 a, blue colored regions) while they were absent in the transcranial condition (no difference for negatively correlated pixels compared to sham sonication, no negative correlations in different pressure conditions). Negative correlations appeared more pronounced with higher frequency but showed a significant effect of pressure on the area of significant negatively correlated pixels in both frequency conditions (1.68 MHz: Friedman test = 0.0104; 4.0 MHz: Friedman test = 0.0003, Supplementary Figure 2).

We found no significant difference between CBV changes in- and off-focus, as well as between regions for FUS neuromodulation with 1.68 MHz, while 4.0 MHz neuromodulation showed significantly stronger increases of CBV in the cortex compared to the deeper brain regions ($p = 0.0228$, respectively; Dunn's test after significant Friedman test ($p = 0.0394$)) and, interestingly, deeper brain regions exhibited CBV decrease (Supplementary Figure 3).

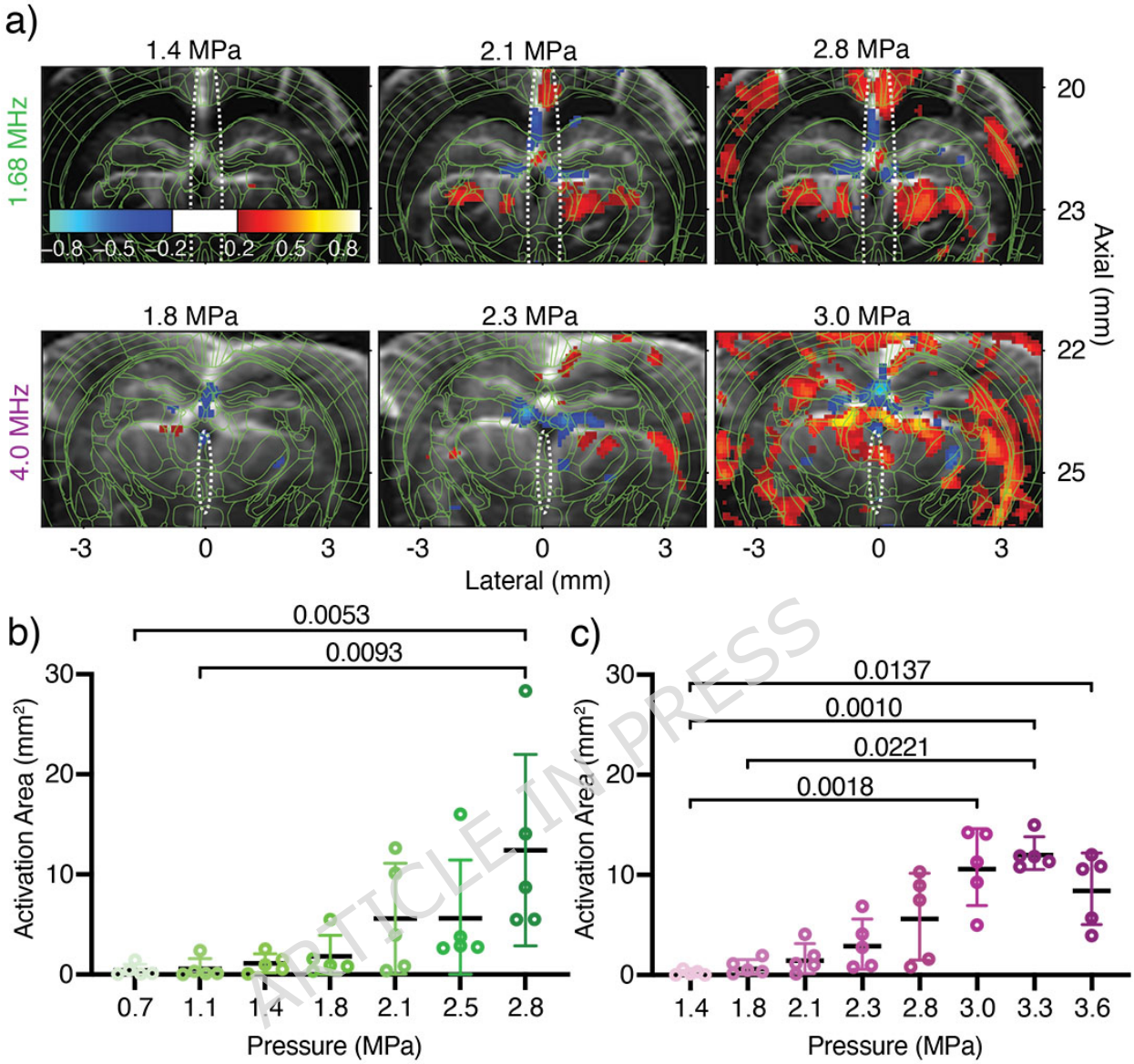

Figure 4. Higher pressures with different center frequencies induce greater activation in craniotomized mice. (a) Representative activity maps of significantly positive correlated pixels (Spearman's $\rho > 0.19$, red hues) and significantly negative correlated pixels (Spearman's $\rho < -0.19$, blue hues) for 2 subjects receiving FUS with 1.68 MHz (upper row, green label) or 4.0 MHz (lower row, purple label) center frequency under different pressure conditions. The predicted acoustic foci (white) assessed during transducer calibration and brain regions (green) are overlaid onto the PDIs. Imaging planes: Upper row AP Bregma -1.4 mm, bottom row AP Bregma -1.7 mm. (b) Area with CBV increases correlated with the FUS stimulus (positively correlated pixels) for different pressures in the 1.68 MHz condition (n = 5 paired trials in 5 mice, median

AP direction of imaging planes: -1.5 mm from Bregma, Range = -1.4 mm to -1.9 mm; Friedman test: $p = 0.0010$). (c) Area with CBV increases correlated with the FUS stimulus for different pressures in the 4.0 MHz condition ($n = 5$ paired trials in 5 mice, median AP direction of imaging planes: -1.5 mm from Bregma, Range = -1.4 mm to -2.0 mm; Friedman test: $p < 0.0001$). Areas of negatively correlated pixels are depicted in Supplementary Figure 3. Data is depicted as individual observations (circles) with mean (central line) and standard deviations (whiskers). Activity maps and color bars show Spearman correlation coefficients. Dunn's test (corrected for multiple comparisons) was used for post-hoc comparisons after significant Friedman tests.

Transcranial FUS induces hemodynamic responses with ipsilateral bias

To investigate if FUS causes lateralized responses, sonications were targeted 1 mm left and right of the midline in each imaging plane in 11 paired trials across 6 subjects. As shown before for FUS neuromodulation along the midline, unilateral sonications produced mostly cortical bilateral hemodynamic responses (Figure 5 a). However, greater areas with significant CBV increases were observed in the ipsilateral sonicated hemisphere (Figure 5 b). In addition, the mean Spearman's ρ was significantly higher in the hemispheres where FUS was delivered compared to the contralateral hemispheres (Figure 5 c).

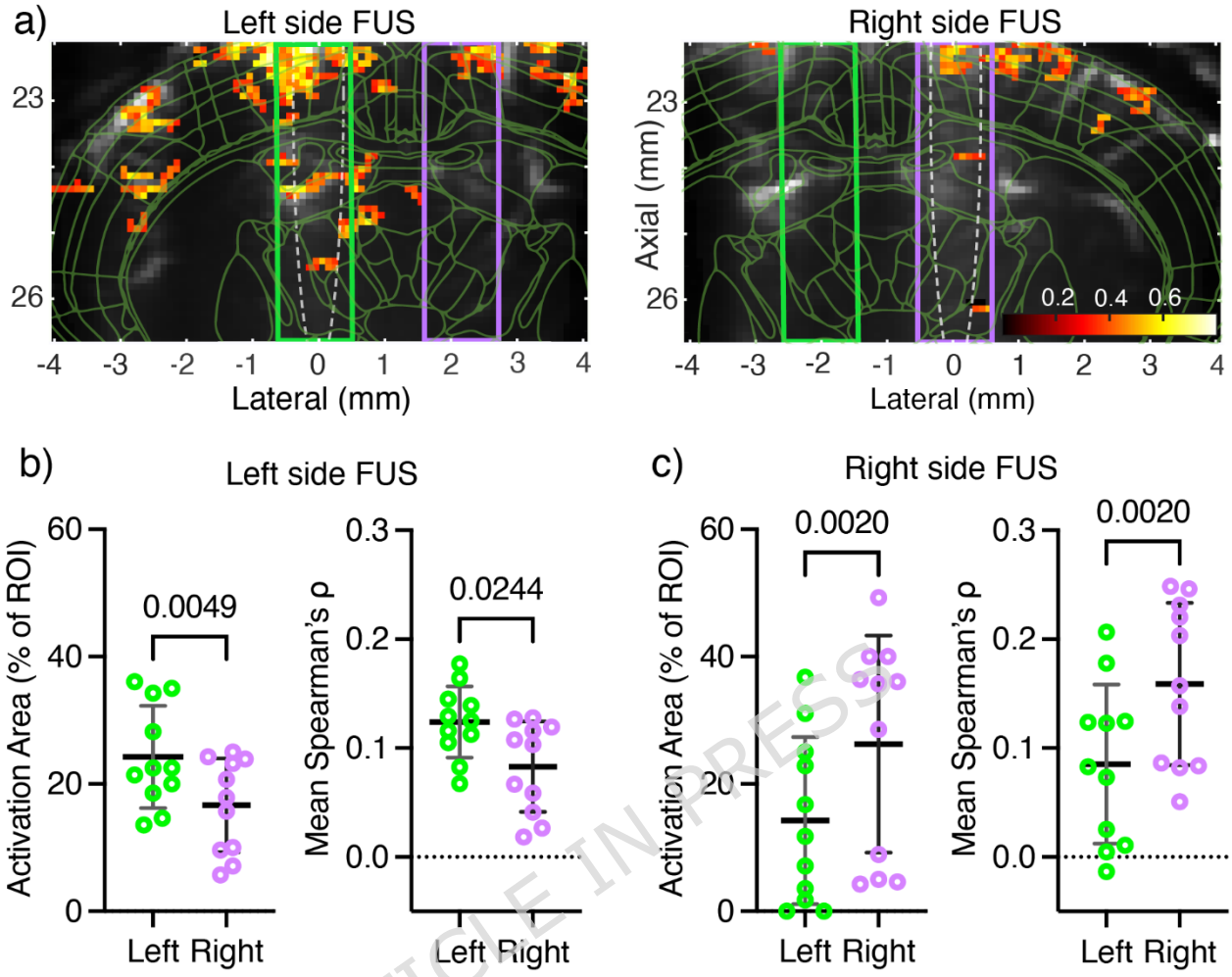

Figure 5. Transcranial FUS (center frequency: 1.68 MHz) shows ipsilateral bias in CBV responses to unilateral sonications. Representative maps of CBV increases significantly correlated with the FUS stimulus (Spearman's $\rho > 0.285$) overlaid onto PDI (grayscale) and brain regions of imaging plane (green) for left **(a**, left side**)** and right **(a**, right side**)** hemispheric sonications at 1.7 MPa derated PNP (n =11 paired trials in 6 mice, median AP direction of imaging planes: -0.5 mm from Bregma, Range = -0.4 mm to -1.3 mm). Rectangles show regions of interest (ROI) in the right (purple) and left (green) hemispheres that were used for analyses in **b** and **c**. The dotted white line shows the predicted acoustic foci (white) assessed during transducer calibration. Activity maps display the full extent of the imaging field of view. FUS induces significantly more pixels with CBV increases correlated with the FUS stimulus and higher mean correlation coefficients in the sonicated ipsilateral ROI compared to the unsonicated contralateral ROI (**b**: left

sonication and **c**: right sonication). Data is depicted as individual observations (circles) with mean (central line) and standard deviations (whiskers). Wilcoxon matched-pairs signed rank test was used for group comparisons. Activity maps and color bars show Spearman correlation coefficients. See Supplementary Figure 4 for activation maps from all individual animals

Safety of transcranial FUS-fUSI

We found no signs of structural changes or blood cell extravasations in H&E staining in n = 2 mice that were sacrificed 24 h following FUS with the highest pressure used for transcranial FUS (center frequency = 1.68 MHz, PNP = 2.6 MPa, Supplementary Figure 5 c/d). Thermocouple measurements (n = 2 mice per target, center frequency = 1.68 MHz) showed maximal temperature increases of 0.81 °C, 1.44 °C or 3.44 °C at –2 mm DV in the brain tissue and 0.70 °C, 2.08 °C or 3.58 °C directly under the skull for derated peak negative pressures of 0.8 MPa, 1.7 MPa and 2.6 MPa, respectively (Supplementary Figure 5 a/b).

Discussion

This study presents the first implementation of transcranial fUSI in combination with transcranial FUS to investigate hemodynamic responses during and following FUS stimulation in the CNS. We demonstrate that higher pressures increase the brain area with significant CBV increases and induce stronger CBV increases, while lateralized sonications result in CBV responses with ipsilateral bias in mice.

Our results demonstrate robust and repeatable bilateral increases in CBV in cortical and subcortical areas during FUS stimulation. Importantly, we did not find a significantly stronger CBV response in the focal area and transcranial FUS resulted mainly in cortical CBV increases. The predominantly cortical distribution of the response in combination with the reduced cortical activation in the cranial window condition points to skull-mediated thermal effects as a major contributor to the widespread hemodynamic changes observed transcranially. Higher FUS

intensities can cause skull heating, and heat transfer from the skull to the cortical surface and meningeal vasculature can induce vasodilation independently of neuronal firing [47,48] and temperature-induced changes in neuronal activity [22]. Thermocouple measurements directly under the skull showed temperature increases of up to 3.58 °C at the highest pressure, consistent with a thermally driven cortical CBV response. This interpretation is further supported by the observation that at 0.8 MPa, transcranial FUS produced a reliable cortical activation, while no activation was observed at 1.4 MPa in a cranial window setup. Another explanation for this observation could be differences in baseline temperature between the two models, because the contact with ultrasound gel decreases temperatures in more superficial brain regions, which is more pronounced the cranial window model (see Supplementary Figure 6 and discussion below). Additional skull-related mechanisms, including intracranial reverberations generating off-target pressure amplitudes [20], may further contribute to the widespread activation pattern. While skull-mediated effects appear to be a dominant mechanism, we cannot exclude contributions from network-associated neuronal activations. Our group and others have previously demonstrated off-target activations potentially associated with connected brain regions [45,49] and network-associated changes in functional connectivity following FUS neuromodulation have been reported [50–53]. The long neuromodulation periods (20 s) and high pressures employed in this study make it conceivable that connected brain areas were activated, while the comparatively low frame rate of fUSI did not allow the identification of a focal starting point. The consistent responses at single transducer positions, the smaller activated area with the smaller focus, and the ipsilateral bias in lateralized sonications would be compatible with a network-level contribution. However, the ipsilateral bias could also be explained by a heating-based mechanism, because hemisphere closest

to the sonicated region of the skull would receive more thermal energy, which could induce stronger CBV responses without requiring network-level neuronal recruitment.

The widespread, non-focal pattern we observe could also be consistent with off-target vascular effects, which have been demonstrated with a variety of different modalities. Single vessel photothrombosis studies have shown that occluding pial arterioles leads to flow redistributions in neighboring downstream branches, with effects detectable across the cortical surface network [54]. Off-target effects after venous perturbations are particularly pronounced and anatomically relevant for the midline sonications in this study. Occlusion of a single ascending or surface venule can cause reversals in flow direction, capillary vasodilation, and blood-flow decreases in upstream capillaries [55]. Because the superior sagittal sinus drains both hemispheres and lies directly beneath the skull at the midline, heating or mechanical effects could potentially induce widely distributed vascular effects consistent with our results. In line with this, a recent optical imaging study has shown that the superior sagittal sinus and bridging veins undergo active contractions tied to respiration, locomotion and abdominal compression and that this mechanism can drive increases in cortical blood flow without neuronal activation [56].

A more recent study from our group that combined fUSI with displacement imaging in an open craniotomy mouse model has demonstrated that the displaced area of brain tissue is larger than the area of the FUS focal spot in the brain and that FUS neuromodulation along the midline can cause bilateral hemodynamic responses [45]. In the same study, the effects of FUS neuromodulation were more focal, but there are several technical differences between the current study and our previous work that likely contribute to the lack of clear focal responses. As previously stated, the presence of the skull can cause skull heating, intracranial reverberations and the lower center frequency of FUS (1.68 MHz in the current vs 4.0 MHz in the previous study) increases the area

of effect and the likelihood of larger network stimulations in the transcranial paradigm. In the cranial window model employed in a part of this study we used the same center frequency as reported in our previous work (4.0 MHz) and still found primarily non-focal responses. This discrepancy could be explained by several key differences: First, in this study we used a cranial window implantation which opens a smaller brain surface area compared to a full craniotomy from our previous study, while adjacent parts of the skull are covered with dental cement and the window with a PMP membrane. This can potentially lead to subtle standing waves on the sides of the bone cement and at the PMP membrane, increasing the likelihood of non-focal activation. Second, the previous study used longer burst durations (300 ms vs 150 ms) and shorter stimulation periods (10 s vs 20 s). The reduction in uninterrupted acoustic energy (burst duration) may fall below the threshold required for robust focal neuronal activation and decrease heating, which likely contributed to the effect in our previous study. The extended stimulation window may favor the detection of cumulative network-level spread and global hemodynamic shifts, which could mask the focal engagement when integrated over the total imaging period. Third, the two studies used different focal targets with the current study primarily targeting more posterior and medial structures and thus a larger area of the thalamus, which is broadly connected to most of the brain, while an anterior medial stimulation in our previous study similarly produced a less focal response than lateral stimulation. Finally, the PNPs employed in the current study were lower than in our previous work (2.23 MPa vs 3.39 MPa for highest PNP) and importantly pressures below 2.54 MPa did not elicit clear focal responses in that earlier study.

The near-absence of activation at 1.4 MPa in the cranial window condition raises an important question about whether this reflects the sensitivity limit of our fUSI setup or a genuine absence of hemodynamic changes at this intensity without skull-mediated effects. In this study, we did not

observe significant CBV changes in response to FUS lower than 1.4 MPa, which is consistent with our previous cranial window work [45]. However, earlier studies using optical imaging [57] and fMRI [5] have reported FUS-evoked changes in CBF or BOLD signals with lower pressures, suggesting that our experimental setup may have lower sensitivity for capturing subtle changes compared to alternative imaging techniques. This limited sensitivity could be a result of the SVD filtering applied to remove tissue signals, which may have inadvertently rejected slow perfusion components that predominantly reflect neurovascular coupling. Another factor could be the anesthetic agent used, since isoflurane anesthesia causes baseline vasodilation [58], which likely reduces the available contrast for detecting FUS-induced CBV changes. Given these limitations, our detection threshold probably prevented observation of subtle hemodynamic effects at conventional low-intensity parameters. Future work with optimized SVD filtering or alternative anesthetic protocols may help resolve whether low-intensity FUS truly lacks vascular effects or whether they simply fall below our current detection capability.

Notably, in the auditory sham condition performed with a cranial window (Figure 1e), activation was observed outside the predicted acoustic focus but not within it, even in the absence of skull heating and reverberation effects. This pattern is consistent with indirect hemodynamic responses propagating through vascular networks rather than direct FUS-induced effects at the focus. The cerebrocortical vasculature is known to redistribute flow rapidly through anastomotic connections following focal perturbations [54,55]. Moreover, the relatively large focal size inherent to our 1.68 MHz transducer may result in acoustic energy deposition extending beyond the theoretically predicted focus, while the peripheral regions of the sonicated field produce detectable vascular responses when the central focus does not. Finally, at the pressure used in this sham condition (2.5 MPa), the primary FUS-induced response at the focus may still be partly below fUSI detection

threshold, while secondary responses in connected vascular territories are amplified and detectable through neurovascular coupling or vascular redistribution mechanisms.

Although we were able to identify widespread and pressure-dependent hemodynamic changes induced by FUS, we did not establish a clear distinction between CBV changes due to neuronal activity or the FUS stimulus acting directly on the vasculature. There is evidence that focal acoustic, optical, or thermal energy can drive vascular responses without engaging neurons. Microbubble-mediated FUS produces vasoconstriction and measurable CBV reductions detectable on ULM and contrast-enhanced power Doppler [59]. Conversely, optical energy deposition can produce reversible vasodilation in mice with fUSI as readout, which is indistinguishable from neurally driven activation [60]. For this reason, further studies that combine fUSI with electrical, optical or histological markers (e.g. cFOS) of neuronal activity in multiple brain regions are warranted to better elucidate the hemodynamic and neuronal effects induced by FUS neuromodulation in the brain. In addition, future work should focus on targeting brain regions with more well-established connectivity to investigate the network-level effects of FUS more clearly.

Subcortical changes in CBV were inconsistent during transcranial fUSI acquisitions while reliable responses were observed in the cortex. In mice implanted with an ultrasound-transparent cranial window, we found more robust changes in CBV in subcortical regions and less pronounced cortical responses. These results could be explained by the effects of temperature on neuronal activation or the vasculature. Thermocouple measurements revealed a baseline temperature of 31.6 °C in the cortex and 33.6 °C in the thalamus in the cranial window condition (Supplementary Figure 6), whereas brain temperature under similar anesthetic conditions without a cranial window has been reported by others to be 34.6 °C or 35.4 °C, respectively [61]. Two-photon imaging through a smaller cranial window with a room-temperature water immersion objective has been shown to

cool the cortex by 2–3 °C and cause a significant drop in resting capillary blood flow and RBC velocity [62]. In addition, temperature has been shown repeatedly to influence neuronal activation and cerebral blood flow [23,63–65]. Specifically, temperature decreases induce lower cerebral blood flow, while the effects on neuronal activity are mostly described as excitatory [23,64]. Furthermore, lower temperature decreases the activity of mechanosensitive channels like Piezo1 [66] and TRPP2 [67] which have been shown to excite neurons during FUS stimulation [68]. These temperature-dependent mechanisms, combined with the skull heating effects discussed above, could explain the differences between the activation profiles in the transcranial and cranial window conditions. Further investigation of the effects of temperature in the context of fUSI and during FUS stimulation is therefore warranted to advance our understanding and refine the application of both techniques. In addition, the stronger cortical hemodynamic responses and less pronounced subcortical response in the transcranial condition compared to animals with a cranial window should caution authors to directly translate results between both cases and carefully adjust relevant parameters like the cranial temperature.

Interestingly, we were able to identify negatively correlated regions with stimulation-associated decreases in CBV in mice implanted with a cranial window, which could be connected to decreases in neuronal activity [69]. Negative BOLD and CBV signals have been attributed to neuronally driven surround inhibition with concurrent vasoconstriction [70,71], to a ‘steal-phenomenon’ [72] in the vicinity of active regions or to vasoconstriction independent of neuronal activity [73]. The absence of negatively correlated regions in the transcranial condition could indicate a lower sensitivity in transcranial imaging. The association of higher frequency with more negatively correlated pixels indicates an effect of frequency or focal size on the hemodynamic responses during FUS that warrants further investigation.

Limitations of this study include comparatively high FUS intensities and temperature increases that far exceed the FDA guidelines for diagnostic ultrasound [74] and ITRUSST recommendations [75] commonly applied in the field of FUS neuromodulation. As discussed above, this study does not allow to distinguish between thermal and mechanical effects on neuronal signals and vascular responses in the brain, especially given that the highest pressures induced temperature increases > 2 °C in the brain and under the skull. In a more recent study by our group, we have demonstrated association of mechanical effects induced by FUS with CBV changes by mapping the displacement induced by the radiation force, which was not performed in this study [45]. Despite this, fUSI was able to pick up FUS-induced hemodynamic changes even in lower pressures that caused less pronounced temperature increases (< 1 °C). Another limitation comes from the variation in the imaging planes used to study the effects of FUS with fUSI, especially in the transcranial condition. This does not allow the precise identification of possible pathways or vascular networks engaged by FUS stimulation. However, the fact that we were able to nevertheless find the demonstrated relationships with FUS pressure and lateral bias of responses could suggest robust effects on wider neuronal or vascular networks. Another limitation is that auditory artifacts could not be completely ruled out as a potential confounder in the hemodynamic activations. This concern is particularly relevant in light of recent research indicating that auditory confounds are a primary factor driving FUS neuromodulation effects in humans [76]. However, the absence of activation in an auditory sham condition, along with the dose-dependent effects and lateralized responses observed with FUS, strongly indicates that the mechanism of action is not predominantly auditory. To conclusively eliminate auditory artifacts, future studies will entail a transgenic, conditionally deafened mouse model, as described by Guo et al. [77].

To conclude, we show that transcranial fUSI can capture region-dependent hemodynamic responses to transcranial FUS and displays stronger responses in higher-pressure conditions. The comparison between transcranial and cranial window conditions suggests that skull-mediated thermal effects are a major contributor to the widespread cortical CBV increases observed transcranially, although contributions from network-level neuronal activation and direct vascular effects cannot be excluded. The pattern of widespread, bilateral, predominantly cortical, non-focal responses we observe is consistent both with skull-mediated mechanisms and with off-target vascular effects of perturbing the dense pial and midline drainage network. Our approach allowed for transcranial imaging of FUS-induced hemodynamic changes with a large field of view in rodents, which could facilitate the study of the mechanisms through which FUS affects brain hemodynamics.

Methods

Animal preparation

The experiments and procedures presented in this study were performed in accordance with the Columbia University Institutional Animal Care and Use Committee. Young male wild-type mice between 8 to 12 weeks of age (C57BL/6, n = 22) were used for transcranial experiments in this study. Animals To assess possible effects of the skull, a subgroup of mice between 8 to 20 weeks of age (C57BL/6, n = 5) was implanted with a chronic cranial window covered by a polymethyl pentene membrane as described by Brunner et al [31]. Mice implanted with a cranial window were allowed to rest for 2 weeks before experiments were performed. Anesthesia was induced with isoflurane (1 - 3%) and supplementary oxygen (0.8 L/min). The absence of a pedal reflex confirmed induction and isoflurane was then decreased and adjusted between 0.5 – 1% to maintain light anesthesia without producing gasping from low oxygenation, to reduce motion artifacts. The

subject's head was fixed by a stereotactic frame (Model 900, David Kopf Instruments, Tujunga, CA, USA) and elastic bands were passed over the body to mitigate motion artifacts. The animal's head was shaved and depilatory cream was used to remove all fur before acoustic gel was placed on the animal's head. Mice with cranial windows were fixed with a 3D-printed holder that connected to the implanted headpost and acoustic gel was placed on the membrane covering the cranial window. A data acquisition system (MP150, Biopac Systems Inc, Goleta, CA) was used to acquire pulse-oximetry signals (MouseOx+, Starr Life Sciences, Oakmont, PA, USA) recorded from a sensor placed on the shaved thigh. The pulse-oximeter was used in conjunction with intermittent toe pinches to monitor the depth of anesthesia. The ideal depth of anesthesia during experiments corresponded with heart rates above 400 bpm and an unresponsive pedal reflex. Following final experiments, animals were euthanized by a combined chemical and physical approach with inhalation of 5% isoflurane until respiratory arrest followed by cervical dislocation. All animal procedures were approved by the Institutional Animal Care and Use Committee at Columbia University (Protocol # AC-AABF2550). and followed the National Institutes of Health guidelines. This study is reported in accordance with the Animal Research: Reporting of In Vivo. Experiments (ARRIVE) guidelines.

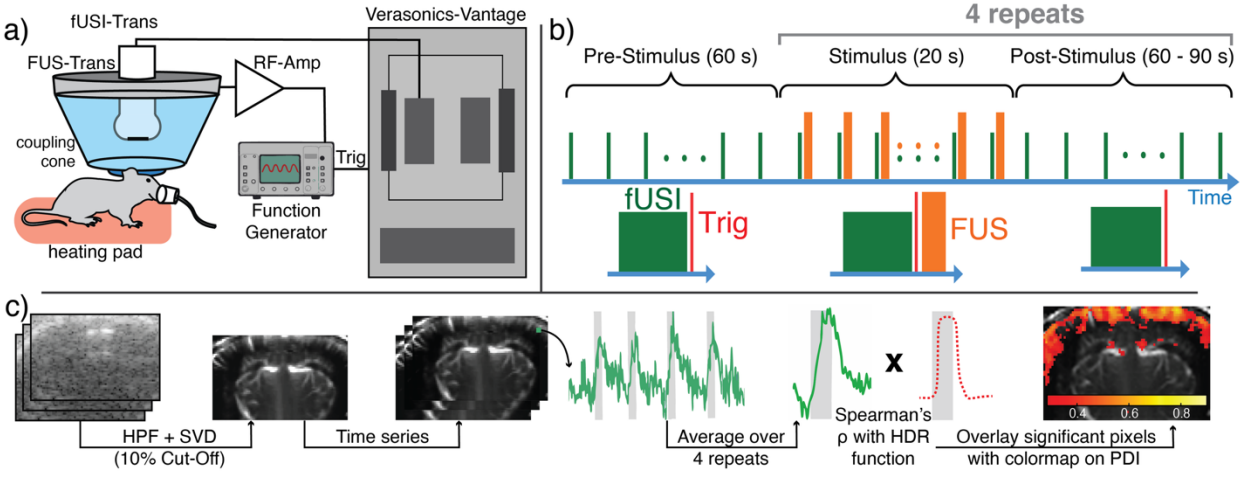

Figure 6. Experimental setup **(a)**, fUSI and FUS stimulus block design **(b)** and fUSI data processing pipeline **(c)**. Abbreviations: FUS – focused ultrasound, fUSI – functional ultrasound, HDR – hemodynamic response, HPF – high pass filter, PDI – power doppler image, RF-Amp – radiofrequency amplifier, SVD – singular value decomposition, Trig – Trigger.

FUS Stimulation

We used single-element spherical segment annular focused ultrasound transducers (H-204 and H-215, Sonic Concepts Inc, Bothell, WA, USA) that were confocally aligned with an ultrasound imaging array (L22-14vXLF, Vermon S.A., Tours, France). The H-204 transducer was operated the 3rd harmonic (1.68 MHz) to achieve a tighter focal volume and allow the identification of focal vs. non-focal effects in the small mouse brain. Each transducer had an acoustic coupling cone attached to the transducer face with an acoustically transparent membrane (Tegaderm, 3M Company, Maplewood, MN, USA) placed over its opening. The sealed coupling chamber was filled with deionized water and degassed using a degassing system (WDS105+; Sonic Concepts, Bothell, WA, USA). FUS transducers were calibrated in a degassed water tank using a hydrophone (HGL0200, Onda Corporation, Sunnyvale, CA, USA) in free field or with ex vivo skulls for estimating attenuation and reporting derated pressures. FUS sequences were driven by a function generator and amplified with an RF amplifier (325LA, Electronics Innovation Ltd., Rochester, NY, USA). A schematic of the setup is depicted in Figure 6 a and the acoustic parameters and focal size of the transducers are listed in Table 1. For targeting, the confocal FUS-fUSI transducer system was lowered into the acoustic gel on the scalp, ensuring that no bubbles were trapped along the beam path. B-mode imaging was used to verify adequate acoustic coupling. Targeting was performed by first landmarking the interaural line using B-mode imaging to locate highly reflective metal syringe tips temporarily placed on the stereotactic ear bars (i.e. interaural line). The syringe tips were then removed, taking care not to leave trapped air bubbles that could result in signal loss

or artifacts. Neuronavigation could then be performed by manually translating the transducer system in the anteroposterior or mediolateral (ML) directions according to a reference atlas [78] using the micromanipulator (David Kopf Instruments, Tujunga, CA, USA). In animals with cranial windows, targeting was performed by using the anterior border of the cranial window (Bregma +2 in the anteroposterior direction) as a reference point and moving the transducer system with a motorized stage. In transcranial experiments, manual positioning of the imaging transducer resulted in natural variation in the anteroposterior (AP) position of the imaging plane across animals, compounded by the approximately 400 μm thickness of the imaging plane in the AP direction. While FUS was consistently targeted in the ML directions, the coronal imaging plane position varied across subjects. This variation was intentionally used in the pressure-dependence experiments (Figure 2a) to demonstrate that FUS-induced hemodynamic effects are consistent across different AP positions. Due to this inter-animal variation in imaging plane position, representative individual maps are presented to illustrate the spatial consistency of pressure-dependent and lateralization effects. We used post-hoc mapping of the power Doppler images based on custom vasculature reference scans relative to Bregma over the whole brains of two mice (0.1 mm steps) and found that the imaging planes used in this work span between -0.2 mm to -2.0 mm from Bregma in the anteroposterior direction. Imaging planes of all figures shown and the median (range) of imaging planes used in datasets can be found in the figure captions. Sonications were performed along the midline (± 0 mm ML) or at ± 1 mm ML to investigate lateralization effects. Given the AP range of imaging planes, sonicated structures encompassed the somatosensory cortex, hippocampus, and thalamus, with the specific anatomical composition depending on the exact AP position of each imaging plane. To mitigate auditory artifacts associated with pulsed ultrasound, we implemented an amplitude-modulated (AM) sequence

[79,80]. The amplitude modulation was based on a sine wave (half cycle) and the energy deposited in the tissue was equal to a duty cycle of 64% (Supplementary Figure 1). A block design was implemented consisting of a 60 s baseline imaging block followed by four 20 s FUS blocks with intervals randomized between 60 and 90 s. During the FUS blocks (20 s), the function generator output was triggered by a programmable research ultrasound system (Vantage 256, Verasonics, Kirkland, WA) immediately after each image acquisition at a frequency of approximately 1 Hz (20 pulses in total). As described previously, this triggering paradigm was chosen to avoid any interference between FUS and fUSI (Figure 6 b) [45].

Table 1. FUS and fUSI equipment and acoustic parameters.

FUS	
Focal Size (-6 dB)	H-204: 0.8 mm (lateral), 8 mm (axial) H-215: 0.3 mm (lateral), 2 mm (axial)
Acoustic Parameters	Carrier Frequency: H-204: 1.68 MHz (3rd Harmonic) H-215: 4 MHz Amplitude Modulation Freq: 1 kHz Burst Duration: 150 ms Sonication Frequency: H-204: 1 Hz H-215: 2 Hz Peak Negative Pressures: 0.8 - 2.6 MPa (Derated: skull, transcranial, H204) 0.7 - 2.8 MPa (Non-derated, Cranial window, H204) 0.96 - 2.23 MPa (Derated: brain tissue, Cranial window, H215) I_{sppa} 19.78 - 208.96 W/cm^2 (Derated: skull, transcranial, H204) 15.15 - 242.35 W/cm^2 (Non-derated, Cranial window, H204) 31.18 - 168.23 W/cm^2 (Derated: brain tissue, Cranial window, H215) I_{spta} (Pulse train): 1.90 - 20.06 W/cm^2 (Derated: skull, transcranial, H204) 1.45 - 23.27 W/cm^2 (Non-derated, Cranial window, H204) 2.99 - 16.15 W/cm^2 (Derated: brain tissue, Cranial window, H215)
Imaging parameters (fUSI)	

Acoustic Parameters	Center frequency: 15.0 MHz Compounded Plane Wave Imaging Plane Angles: 5 (-6° to 6°) Compounded Image Rate: 500 Hz Compounded Images in PDI: 200 (transcranially) 70 (craniotomized)
Filtering	Singular Value Decomposition: 10% of singular values removed High-Pass Filter: Butterworth (2^{nd} order), 8-Hz cutoff frequency

Sham conditions and safety monitoring

To rule out activations unrelated to FUS or connected to auditory artifacts, two sham conditions were implemented. In the first sham condition, the amplifier was turned off and in the second sham condition a 110 dB, 10 kHz tone (square wave) was delivered instead of the FUS stimulus in the same temporal pattern. The tone was generated with an Arduino microcontroller coupled to a speaker (BA735 Digital, Boston Acoustics, Woburn, MA) that was placed 10 cm in front of the mouse's head. Speaker volume was measured at 10 cm distance at the position of the mouse head with the National Institute for Occupational Safety and Health Sound Level Meter App.

To investigate the safety of the FUS parameters, 2 mice were transcranially sonicated with the highest pressures used for transcranial FUS in this study (1.68 MHz, 2.6 MPa) and the remaining parameters as described in Table 1. Mice were sacrificed 24 hours after the end of the sonication, and brain tissue in the focal plane was stained with H&E for histopathological investigation of tissue morphology and possible blood extravasation. In addition, transcranial temperature measurements were performed in 2 separate mice in two locations by placing a thermocouple (HYP1, T-type needle thermocouple, 0.25 mm diameter, Omega Engineering, Norwalk, CT) directly under the skull or at the estimated location of the center of the FUS focus in the brain with a micromanipulator. At each location, the thermal response was maximized by micromanipulation

of the focus in the anteroposterior and mediolateral direction in 0.1 mm steps. FUS pulses with 1.68 MHz were delivered with 0.8, 1.7 and 2.6 MPa for a total duration of 20 s with the parameters described in Table 1. Temperature measurements were corrected for the viscous heating artifact by iterative curve fitting of the Bioheat Transfer Equation as described previously [81].

Functional Ultrasound Imaging (fUSI)

fUSI was implemented to detect and characterize stimulus-evoked hemodynamic changes in the mouse brain. The imaging sequence was generated using a programmable research ultrasound system to perform ultrafast compounded plane wave imaging. fUSI was performed by acquiring a time series of coronal power Doppler images (PDI) at a resolution of 103 μm, assuming a sound speed of 1546 m/s for brain tissue. The effective temporal resolution of our fUSI setup was approximately 1 s (one compound Power Doppler frame per second), which is typical for fUSI implementations that generally achieve temporal resolutions on the order of hundreds of milliseconds. Array specifications and imaging parameters utilized are provided in Table 1. A single compounded image was generated by averaging delay-and-sum reconstructed ultrasound images acquired from multiple plane wave transmits. A PDI was generated by first applying a high-pass filter to a stack of compounded images followed by spatiotemporal filtering using singular value decomposition (SVD), where the upper 10% of eigenvalues were discarded to filter out tissue clutter signal [37,38]. SVD filtering cannot remove the influence of large motion artifacts, so outlier frames were removed whose mean image value was three standard deviations above the mean image value of the remaining image set. The pixel intensity data, representing CBV, was averaged across the four stimuli before performing the statistical analysis. The image processing steps are outlined in Figure 6 c.

Correlation Analysis

Statistical analyses were performed to identify pixels exhibiting intensity time courses that were significantly correlated with applied stimulus patterns as described previously [42]. The binary stimulus vector (i.e. FUS ON vs FUS OFF) was convolved with a modified hemodynamic response function (HRF) [31] to generate a more physiologically relevant HRF regressor for computing correlation coefficients. The following parameters were used: delay of response (relative to onset) = 4 s, delay of undershoot (relative to onset) = 36 s, dispersion of response = 0.5, dispersion of undershoot = 1, ratio of response to undershoot = 20, onset = 0 s, length of kernel (seconds) = 16 s. Pixel-wise Spearman correlation coefficients were then computed between the regressor and PDI time series. Pixels were defined as showing a significant correlation with the FUS stimulus with $\rho > 0.29$ (transcranial experiments) or $\rho > 0.19$ (craniotomized experiments). The thresholds were obtained as described by Brunner et al. [31] by using Fisher's transform with $Z = 2.58$ ($p < 0.01$) for 80 or 175 time points, respectively. Significantly correlated pixels were used to create binary maps. The computed correlation values were then remapped using the binary maps to be overlaid onto the mean PDI (Figure 6 c). Correlation maps were filtered in space with a median filter (kernel size = 3) and CBV response curves were filtered with a rolling mean (window size = 3) before being displayed. A significant hemodynamic response was defined as a condition in which the area of CBV increases significantly correlated with the FUS stimulus was significantly different from zero (based on one-sample t-test comparing the area of significantly correlated pixels against 0). This definition ensures that only spatially extensive, stimulus-locked hemodynamic changes exceeding our detection thresholds are classified as significant responses.

Analysis of CBV changes in- and off-focus

To analyze the CBV changes in different brain regions in and off-focus, three regions of interest (ROIs) were defined to include (1) all cortical areas; (2) hippocampus, fimbria and ventral

hippocampal commissure; (3) thalamus and hypothalamus. The ROIs were manually drawn over the regions based on the Allen Mouse Brain Atlas [46] and the Power Doppler Images. The mean of all pixels in- or off-focus in the respective ROIs was calculated to allow comparisons between the longitudinal changes in CBV over time. Statistical analysis between regions and in- and off-focus activity was performed on mean CBV changes during the FUS neuromodulation period (20 s).

Data Availability

Datasets and executable codes can be shared by the corresponding author upon reasonable request.

Declaration of competing interest

The authors declare that they have no known competing financial interests or personal relationships that could have appeared to influence the work reported in this paper.

CRediT authorship contribution statement

Jonas Bendig: Conceptualization, Formal analysis, Investigation, Methodology, Project administration, Visualization, Writing – original draft, Writing – review & editing. **Christian Aurup:** Conceptualization, Formal analysis, Investigation, Methodology, Project administration, Software, Visualization, Writing – original draft, Writing – review & editing. **Samuel G. Blackman:** Software, Visualization, Writing – review & editing. **Erica P. McCune:** Visualization, Writing – review & editing. **Seongyeon Kim:** Project administration, Software, Writing – review & editing. **Elisa E. Konofagou:** Conceptualization, Funding acquisition, Methodology, Supervision, Writing – original draft, Writing – review & editing.

Acknowledgments

We would like to thank Dr. Stephen Lee for his crucial advice and support during the whole project.

Funding

This work was supported by the National Institutes of Health (Award numbers: 5R01EB02757 6-04 and 5R01AG03896 1-10) and Jonas Bendig was partially supported by the Thiemann Foundation and the German Research Foundation.

References

1. Hameroff, S. *et al.* Transcranial ultrasound (TUS) effects on mental states: a pilot study. *Brain Stimulat.* **6**, 409–415 (2013).

2. Tufail, Y. *et al.* Transcranial pulsed ultrasound stimulates intact brain circuits. *Neuron* **66**, 681–694 (2010).

3. Tufail, Y., Yoshihiro, A., Pati, S., Li, M. M. & Tyler, W. J. Ultrasonic neuromodulation by brain stimulation with transcranial ultrasound. *Nat. Protoc.* **6**, 1453–1470 (2011).

4. Murphy, K. R. *et al.* A tool for monitoring cell type-specific focused ultrasound neuromodulation and control of chronic epilepsy. *Proc. Natl. Acad. Sci. U. S. A.* **119**, e2206828119 (2022).

5. Yoo, S.-S. *et al.* Focused ultrasound modulates region-specific brain activity. *Neuroimage* **56**, 1267–1275 (2011).

6. Yu, K., Niu, X., Krook-Magnuson, E. & He, B. Intrinsic functional neuron-type selectivity of transcranial focused ultrasound neuromodulation. *Nat. Commun.* **12**, 2519 (2021).

7. Fry, F. J., Ades, H. W. & Fry, W. J. Production of reversible changes in the central nervous system by ultrasound. *Science* **127**, 83–84 (1958).

8. Sarica, C. *et al.* Human Studies of Transcranial Ultrasound neuromodulation: A systematic review of effectiveness and safety. *Brain Stimulat.* **15**, 737–746 (2022).

9. Kamimura, H. A. S., Conti, A., Toschi, N. & Konofagou, E. E. Ultrasound neuromodulation: mechanisms and the potential of multimodal stimulation for neuronal function assessment. *Front. Phys.* **8**, 150 (2020).

10. Li, D. *et al.* Low-Intensity Pulsed Ultrasound Dynamically Modulates the Migration of BV2 Microglia. *Ultrasound Med. Biol.* **51**, 494–507 (2025).

11. Leinenga, G. & Götz, J. Scanning ultrasound removes amyloid-β and restores memory in an Alzheimer's disease mouse model. *Sci. Transl. Med.* **7**, 278ra33 (2015).

12. Mishima, T. *et al.* Repetitive pulsed-wave ultrasound stimulation suppresses neural activity by modulating ambient GABA levels via effects on astrocytes. *Front. Cell. Neurosci.* **18**, 1361242 (2024).

13. Kim, E. *et al.* Non-invasive measurement of hemodynamic change during 8 MHz transcranial focused ultrasound stimulation using near-infrared spectroscopy. *BMC Neurosci.* **20**, 12 (2019).

14. Shen, Y. Y. *et al.* Label free, capillary-scale blood flow mapping in vivo reveals that low-intensity focused ultrasound evokes persistent dilation in cortical microvasculature. *Commun. Biol.* **8**, 12 (2025).

15. Murphy, K. R. *et al.* Optimized ultrasound neuromodulation for non-invasive control of behavior and physiology. *Neuron* https://doi.org/10.1016/j.neuron.2024.07.002 (2024) doi:10.1016/j.neuron.2024.07.002.

16. Estrada, H. *et al.* High-resolution fluorescence-guided transcranial ultrasound mapping in the live mouse brain. *Sci. Adv.* **7**, eabi5464 (2021).

17. Estrada, H. *et al.* Holographic transcranial ultrasound neuromodulation enhances stimulation efficacy by cooperatively recruiting distributed brain circuits. *Nat. Biomed. Eng.* https://doi.org/10.1038/s41551-025-01449-x (2025) doi:10.1038/s41551-025-01449-x.

18. Kamimura, H. A. S. *et al.* Focused ultrasound neuromodulation of cortical and subcortical brain structures using 1.9 MHz. *Med. Phys.* **43**, 5730 (2016).

19. Yang, Y. *et al.* Induction of a torpor-like hypothermic and hypometabolic state in rodents by ultrasound. *Nat. Metab.* **5**, 789–803 (2023).

20. Aurup, C., Kamimura, H. A. S. & Konofagou, E. E. High-Resolution Focused Ultrasound Neuromodulation Induces Limb-Specific Motor Responses in Mice in Vivo. *Ultrasound Med. Biol.* **47**, 998–1013 (2021).

21. Darrow, D. P., O'Brien, P., Richner, T. J., Netoff, T. I. & Ebbini, E. S. Reversible neuroinhibition by focused ultrasound is mediated by a thermal mechanism. *Brain Stimulat.* **12**, 1439–1447 (2019).

22. Bendau, E. V. *et al.* Modulation of cardio-respiratory activity in mice via transcranial focused ultrasound. *Ultrasound Med. Biol.* **50**, 332–340 (2024).

23. Kim, T. *et al.* Thermal effects on neurons during stimulation of the brain. *J. Neural Eng.* **19**, 056029 (2022).

24. Constans, C., Mateo, P., Tanter, M. & Aubry, J.-F. Potential impact of thermal effects during ultrasonic neurostimulation: retrospective numerical estimation of temperature elevation in seven rodent setups. *Phys. Med. Biol.* **63**, 025003 (2018).

25. Ahrens, E. T. & Dubowitz, D. J. Peripheral somatosensory fMRI in mouse at 11.7 T. *NMR Biomed.* **14**, 318–324 (2001).

26. Bosshard, S. C. *et al.* Assessment of brain responses to innocuous and noxious electrical forepaw stimulation in mice using BOLD fMRI. *Pain* **151**, 655–663 (2010).

27. Deffieux, T., Demene, C., Pernot, M. & Tanter, M. Functional ultrasound neuroimaging: a review of the preclinical and clinical state of the art. *Curr. Opin. Neurobiol.* **50**, 128–135 (2018).

28. Martinez de Paz, J. M. & Macé, E. Functional ultrasound imaging: A useful tool for functional connectomics? *NeuroImage* **245**, 118722 (2021).

29. Montaldo, G., Urban, A. & Macé, E. Functional Ultrasound Neuroimaging. *Annu. Rev. Neurosci.* **45**, 491–513 (2022).

30. Urban, A. *et al.* Real-time imaging of brain activity in freely moving rats using functional ultrasound. *Nat. Methods* **12**, 873–878 (2015).

31. Brunner, C. *et al.* Whole-brain functional ultrasound imaging in awake head-fixed mice. *Nat. Protoc.* **16**, 3547–3571 (2021).

32. Macé, E. *et al.* Functional ultrasound imaging of the brain. *Nat. Methods* **8**, 662–664 (2011).

33. Ionescu, T. M., Grohs-Metz, G. & Hengerer, B. Functional ultrasound detects frequency-specific acute and delayed S-ketamine effects in the healthy mouse brain. *Front. Neurosci.* **17**, 1177428 (2023).

34. Rabut, C. *et al.* Pharmaco-fUS: Quantification of pharmacologically-induced dynamic changes in brain perfusion and connectivity by functional ultrasound imaging in awake mice. *NeuroImage* **222**, 117231 (2020).

35. Rabut, C. *et al.* 4D functional ultrasound imaging of whole-brain activity in rodents. *Nat. Methods* **16**, 994–997 (2019).

36. Osmanski, B.-F., Pezet, S., Ricobaraza, A., Lenkei, Z. & Tanter, M. Functional ultrasound imaging of intrinsic connectivity in the living rat brain with high spatiotemporal resolution. *Nat. Commun.* **5**, 5023 (2014).

37. Baranger, J. *et al.* Adaptive Spatiotemporal SVD Clutter Filtering for Ultrafast Doppler Imaging Using Similarity of Spatial Singular Vectors. *IEEE Trans. Med. Imaging* **37**, 1574–1586 (2018).

38. Demené, C. *et al.* Spatiotemporal Clutter Filtering of Ultrafast Ultrasound Data Highly Increases Doppler and fUltrasound Sensitivity. *IEEE Trans. Med. Imaging* **34**, 2271–2285 (2015).

39. Claron, J. *et al.* Co-variations of cerebral blood volume and single neurons discharge during resting state and visual cognitive tasks in non-human primates. *Cell Rep.* **42**, 112369 (2023).

40. Nunez-Elizalde, A. O. *et al.* Neural correlates of blood flow measured by ultrasound. *Neuron* **110**, 1631-1640.e4 (2022).

41. Mace, E. *et al.* Functional ultrasound imaging of the brain: theory and basic principles. *IEEE Trans. Ultrason. Ferroelectr. Freq. Control* **60**, 492–506 (2013).

42. Aurup, C., Pouliopoulos, A. N., Kwon, N., Murillo, M. F. & Konofagou, E. E. Evaluation of Non-invasive Optogenetic Stimulation with Transcranial Functional Ultrasound Imaging. *Ultrasound Med. Biol.* **49**, 908–917 (2023).

43. Bertolo, A. *et al.* Whole-Brain 3D Activation and Functional Connectivity Mapping in Mice using Transcranial Functional Ultrasound Imaging. *J. Vis. Exp. JoVE* https://doi.org/10.3791/62267 (2021) doi:10.3791/62267.

44. Tiran, E. *et al.* Transcranial Functional Ultrasound Imaging in Freely Moving Awake Mice and Anesthetized Young Rats without Contrast Agent. *Ultrasound Med. Biol.* **43**, 1679–1689 (2017).

45. Kim, S., Kwon, N., Hossain, M. M., Bendig, J. & Konofagou, E. E. Displacement and functional ultrasound (fUS) imaging of displacement-guided focused ultrasound (FUS) neuromodulation in mice. *NeuroImage* **298**, 120768 (2024).

46. Wang, Q. *et al.* The Allen Mouse Brain Common Coordinate Framework: A 3D Reference Atlas. *Cell* **181**, 936-953.e20 (2020).

47. Kim, C. *et al.* Closed-loop trans-skull ultrasound hyperthermia leads to improved drug delivery from thermosensitive drugs and promotes changes in vascular transport dynamics in brain tumors. *Theranostics* **11**, 7276–7293 (2021).

48. Blackmore, D. G. *et al.* Low-intensity ultrasound restores long-term potentiation and memory in senescent mice through pleiotropic mechanisms including NMDAR signaling. *Mol. Psychiatry* **26**, 6975–6991 (2021).

49. Yang, P.-F. *et al.* Bidirectional and state-dependent modulation of brain activity by transcranial focused ultrasound in non-human primates. *Brain Stimulat.* **14**, 261–272 (2021).

50. Yaakub, S. N. *et al.* Transcranial focused ultrasound-mediated neurochemical and functional connectivity changes in deep cortical regions in humans. *Nat. Commun.* **14**, 5318 (2023).

51. Folloni, D. *et al.* Manipulation of Subcortical and Deep Cortical Activity in the Primate Brain Using Transcranial Focused Ultrasound Stimulation. *Neuron* **101**, 1109-1116.e5 (2019).

52. Verhagen, L. *et al.* Offline impact of transcranial focused ultrasound on cortical activation in primates. *eLife* **8**, e40541 (2019).

53. Sanguinetti, J. L. *et al.* Transcranial Focused Ultrasound to the Right Prefrontal Cortex Improves Mood and Alters Functional Connectivity in Humans. *Front. Hum. Neurosci.* **14**, 52 (2020).

54. Schaffer, C. B. *et al.* Two-photon imaging of cortical surface microvessels reveals a robust redistribution in blood flow after vascular occlusion. *PLoS Biol.* **4**, e22 (2006).

55. Nguyen, J., Nishimura, N., Fetcho, R. N., Iadecola, C. & Schaffer, C. B. Occlusion of cortical ascending venules causes blood flow decreases, reversals in flow direction, and vessel dilation in upstream capillaries. *J. Cereb. Blood Flow Metab. Off. J. Int. Soc. Cereb. Blood Flow Metab.* **31**, 2243–2254 (2011).

56. Zhang, Q. *et al.* Ultrafast venous and sagittal sinus constrictions in the brain driven by abdominal pressure. 2026.05.02.722426 Preprint at https://doi.org/10.64898/2026.05.02.722426 (2026).

57. Yuan, Y., Wang, Z., Liu, M. & Shoham, S. Cortical hemodynamic responses induced by low-intensity transcranial ultrasound stimulation of mouse cortex. *NeuroImage* **211**, 116597 (2020).

58. Sullender, C. T., Richards, L. M., He, F., Luan, L. & Dunn, A. K. Dynamics of isoflurane-induced vasodilation and blood flow of cerebral vasculature revealed by multi-exposure speckle imaging. *J. Neurosci. Methods* **366**, 109434 (2022).

59. Bae, S. *et al.* Ultrasound flow imaging for assessing cerebrovascular changes following focused-ultrasound blood-brain barrier opening. *Theranostics* **15**, 10028–10044 (2025).

60. Rungta, R. L., Osmanski, B.-F., Boido, D., Tanter, M. & Charpak, S. Light controls cerebral blood flow in naive animals. *Nat. Commun.* **8**, 14191 (2017).

61. Shirey, M. J. *et al.* Brief anesthesia, but not voluntary locomotion, significantly alters cortical temperature. *J. Neurophysiol.* **114**, 309–322 (2015).

62. Roche, M. *et al.* In vivo imaging with a water immersion objective affects brain temperature, blood flow and oxygenation. *eLife* **8**, e47324 (2019).

63. Kiyatkin, E. A. Brain temperature and its role in physiology and pathophysiology: Lessons from 20 years of thermorecording. *Temp. Multidiscip. Biomed. J.* **6**, 271–333 (2019).

64. Van Hook, M. J. Temperature effects on synaptic transmission and neuronal function in the visual thalamus. *PLoS ONE* **15**, e0232451 (2020).

65. Wang, H. *et al.* Brain temperature and its fundamental properties: a review for clinical neuroscientists. *Front. Neurosci.* **8**, (2014).

66. Zheng, W., Nikolaev, Y. A., Gracheva, E. O. & Bagriantsev, S. N. Piezo2 integrates mechanical and thermal cues in vertebrate mechanoreceptors. *Proc. Natl. Acad. Sci. U. S. A.* **116**, 17547–17555 (2019).

67. Ng, L. C. T., Vien, T. N., Yarov-Yarovoy, V. & DeCaen, P. G. Opening TRPP2 (PKD2L1) requires the transfer of gating charges. *Proc. Natl. Acad. Sci. U. S. A.* **116**, 15540–15549 (2019).

68. Yoo, S., Mittelstein, D. R., Hurt, R. C., Lacroix, J. & Shapiro, M. G. Focused ultrasound excites cortical neurons via mechanosensitive calcium accumulation and ion channel amplification. *Nat. Commun.* **13**, 493 (2022).

69. Macé, É. *et al.* Whole-Brain Functional Ultrasound Imaging Reveals Brain Modules for Visuomotor Integration. *Neuron* **100**, 1241-1251.e7 (2018).

70. Shmuel, A., Augath, M., Oeltermann, A. & Logothetis, N. K. Negative functional MRI response correlates with decreases in neuronal activity in monkey visual area V1. *Nat. Neurosci.* **9**, 569–577 (2006).

71. Devor, A. *et al.* Suppressed neuronal activity and concurrent arteriolar vasoconstriction may explain negative blood oxygenation level-dependent signal. *J. Neurosci. Off. J. Soc. Neurosci.* **27**, 4452–4459 (2007).

72. Harel, N., Lee, S.-P., Nagaoka, T., Kim, D.-S. & Kim, S.-G. Origin of negative blood oxygenation level-dependent fMRI signals. *J. Cereb. Blood Flow Metab. Off. J. Int. Soc. Cereb. Blood Flow Metab.* **22**, 908–917 (2002).

73. Shih, Y.-Y. I. *et al.* A new scenario for negative functional magnetic resonance imaging signals: endogenous neurotransmission. *J. Neurosci. Off. J. Soc. Neurosci.* **29**, 3036–3044 (2009).

74. Health, C. for D. and R. Marketing Clearance of Diagnostic Ultrasound Systems and Transducers. https://www.fda.gov/regulatory-information/search-fda-guidance-documents/marketing-clearance-diagnostic-ultrasound-systems-and-transducers (2023).

75. Aubry, J.-F. *et al.* ITRUSST Consensus on Biophysical Safety for Transcranial Ultrasonic Stimulation. Preprint at https://doi.org/10.48550/arXiv.2311.05359 (2024).

76. Kop, B. R. *et al.* Auditory confounds can drive online effects of transcranial ultrasonic stimulation in humans. *eLife* **12**, RP88762 (2024).

77. Guo, H. *et al.* Effects of focused ultrasound in a 'clean' mouse model of ultrasonic neuromodulation. *iScience* **26**, 108372 (2023).

78. Paxinos, G. & Franklin, K. *Paxinos and Franklin's the Mouse Brain in Stereotaxic Coordinates*. (Elsevier Academic Press, 2019).

79. Sato, T., Shapiro, M. G. & Tsao, D. Y. Ultrasonic Neuromodulation Causes Widespread Cortical Activation via an Indirect Auditory Mechanism. *Neuron* **98**, 1031-1041.e5 (2018).

80. Guo, H. *et al.* Ultrasound Produces Extensive Brain Activation via a Cochlear Pathway. *Neuron* **98**, 1020-1030.e4 (2018).

81. Kamimura, H. A. S. *et al.* Iterative Curve Fitting of the Bioheat Transfer Equation for Thermocouple-Based Temperature Estimation In Vitro and In Vivo. *IEEE Trans. Ultrason. Ferroelectr. Freq. Control* **67**, 70–80 (2020).